Article

Role of Host Layer Flexibility in DNA Guest Intercalation Revealed by Computer Simulation of Layered Nanomaterials

Mary-Ann Thyveetil, Peter V. Coveney, H. Christopher Greenwell, and James L. Suter

J. Am. Chem. Soc., **2008**, 130 (37), 12485-12495 • DOI: 10.1021/ja8037068 • Publication Date (Web): 23 August 2008

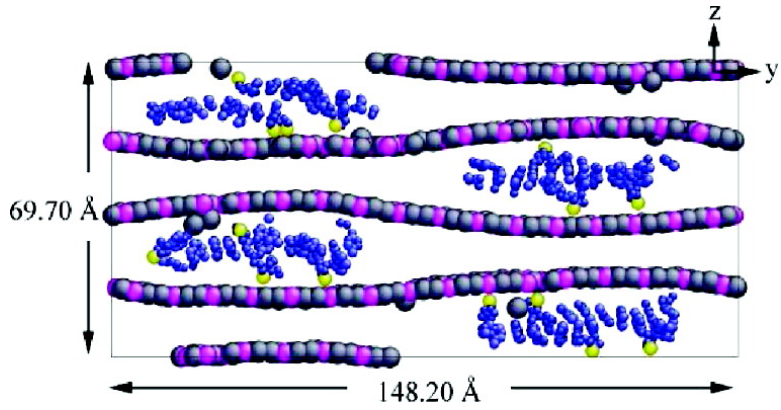

More About This Article

Additional resources and features associated with this article are available within the HTML version:

- Supporting Information
- Access to high resolution figures
- Links to articles and content related to this article
- Copyright permission to reproduce figures and/or text from this article

View the Full Text HTML

J|A|C|S
ARTICLES

Published on Web 08/23/2008

Role of Host Layer Flexibility in DNA Guest Intercalation Revealed by Computer Simulation of Layered Nanomaterials

Mary-Ann Thyveetil, Peter V. Coveney,* H. Christopher Greenwell,† and James L. Suter

Centre for Computational Science, Department of Chemistry, University College London, 20 Gordon Street, London WC1H 0AJ, United Kingdom

Received May 19, 2008; E-mail: p.v.coveney@ucl.ac.uk

Abstract: Layered double hydroxides (LDHs) have been shown to form staged intermediate structures in experimental studies of intercalation. However, the mechanism by which staged structures are produced remains undetermined. Using molecular dynamics simulations, we show that LDHs are flexible enough to deform around bulky intercalants such as deoxyribonucleic acid (DNA). The flexibility of layered materials has previously been shown to affect the pathway by which staging occurs. We explore three possible intermediate structures which may form during intercalation of DNA into Mg_2Al LDHs and study how the models differ energetically. When DNA strands are stacked directly on top of each other, the LDH system has a higher potential energy than when they are stacked in a staggered or interstratified structure. It is generally thought that staged intercalation occurs through a Daumas−Hérold or a Rüdorff model. We find, on average, greater diffusion coefficients for DNA strands in a Daumas−Hérold configuration compared to a Rüdorff model and a stage-1 structure. Our simulations provide evidence for the presence of peristaltic modes of motion within Daumas−Hérold configurations. This is confirmed by spectral analysis of the thickness variation of the basal spacing. Peristaltic modes are more prominent in the Daumas−Hérold structure compared to the Rüdorff and stage-1 structures and support a mechanism by means of which bulky intercalated molecules such as DNA rapidly diffuse within an LDH interlayer.

1. Introduction

The intercalation dynamics of layered materials, such as graphite, clays, and transition-metal dichalcogenides, has been examined in detail, both experimentally[1] and theoretically.[2−4] In particular, the phenomenon of staging has generated a large amount of interest in these materials. Staging is a process by which layered host materials intercalate guest compounds. A staged layered compound has a regularly repeating series of interlayers, which are periodically alternately occupied by intercalant. The length of the period is denoted by the "stage" of the compound (see Figure 1). By way of example, stage-1 compounds have guest intercalants in every interlayer (sometimes called the gallery region), stage-2 compounds have guest intercalants in every other interlayer, and stage-3 compounds have intercalants occupying every third interlayer space. During the full intercalation process, a system may move from a higher order staged structure to a lower one, for example from stage-2 to stage-1, until intercalation is completed. Staging has been most widely described in graphite intercalation compounds, but recent studies of layered double hydroxides (LDHs) also report the formation of intermediary staged structures during intercalation.[5−10]

In LDHs, several species can coexist within the interlayer region. Like clay minerals, LDHs adsorb water as well as charge-balancing counterions; therefore, the process and factors which affect staging in LDHs are also affected by hydration, unlike graphite intercalation compounds.[9] Ordered interstratification has been experimentally observed for terephthalate ions.[11,12] As a result of molecular modeling, Newman et al.[11] suggested that an unequal distribution of water molecules per counterion within an interlayer region leads to interstratification, hence a stage-2 system. In the absence of interlayer water, the rigid terephthalate ions lie horizontally along the basal plane, while in a more hydrated state, the ions stand vertically within

† Present address: Department of Chemistry, Durham University, South Road, Durham DH1 3LE, UK.

(1) Ohzuku, T.; Iwakoshi, Y.; Sawai, K. *J. Electrochem. Soc.* **1993**, *140*, 2490–2498.
(2) Safran, S. A.; Hamann, D. R. *Phys. Rev. Lett.* **1979**, *42*, 1410–1413.
(3) Schon, J. C.; Adler, D.; Dresselhaus, G. *J. Phys. C* **1988**, *21*, 5595–5614.
(4) Ulloa, S. E.; Kirczenow, G. *Phys. Rev. Lett.* **1985**, *55*, 218–221.
(5) Pisson, J.; Taviot-Gueho, C.; Israeli, Y.; Leroux, F.; Munsch, P.; Itie, J.-P.; Briois, V.; Morel-Desrosiers, N.; Besse, J.-P. *J. Phys. Chem. B* **2003**, *107*, 9243–9248.
(6) O'Hare, D.; Evans, J. S. O.; Fogg, A.; O'Brien, S. *Polyhedron* **2000**, *19*, 297–305.
(7) Iyi, N.; Kurashima, K.; Fujita, T. *Chem. Mater.* **2002**, *14*, 583–589.
(8) Taviot-Gueho, C.; Leroux, F.; Payen, C.; Besse, J.-P. *Appl. Clay Sci.* **2005**, *28*, 111–120.
(9) Iyi, N.; Fujii, K.; Okamoto, K.; Sasaki, T. *Appl. Clay Sci.* **2007**, *35*, 218–227.
(10) Williams, G. R.; Norquist, A. J.; O'Hare, D. *Chem. Mater.* **2004**, *16*, 975–981.
(11) Newman, S. P.; Williams, S. J.; Coveney, P. V.; Jones, W. *J. Phys. Chem. B* **1998**, *102*, 6710–6719.
(12) Greenwell, H. C.; Jones, W.; Coveney, P. V.; Stackhouse, S. *J. Mater. Chem.* **2006**, *16*, 708–723.

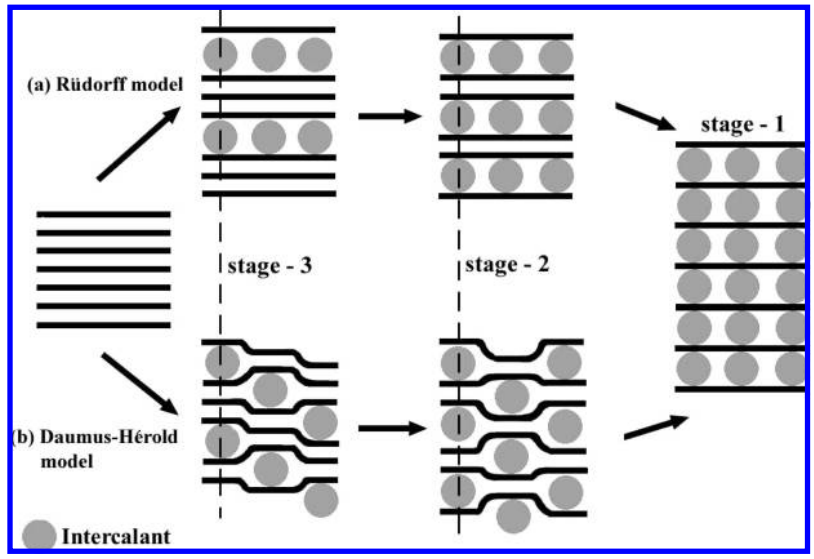

Figure 1. Schematic representation of the possible pathways by means of which layered materials could intercalate ionic species. LDHs are believed to form stage-2 intermediates through a Rüdorff model (a). More flexible materials such as graphite are believed to follow a Daumas−Hérold pathway (b). Our simulations show that Mg_2Al LDHs are able to distort due to the size difference between intercalated DNA and chloride ions, supporting a Daumas−Hérold pathway for intercalation of large biomolecules. The dashed lines indicate similarly staged areas in the two pathways.

the interlayer.[11] Greenwell and Coveney[13] suggested that interstratification of terephthalate ions appeared upon initial formation; galleries may alternately contain different numbers of terephthalate ions.

The process of staging is not completely understood; the small basal spacing of the layered materials investigated makes it difficult to obtain conclusive experimental understanding of the intercalation dynamics. The two main pathways proposed to explain the phenomenon are the Rüdorff[14] and Daumas−Hérold models.[15] The Rüdorff model predicts that staging occurs through the complete intercalation of alternating galleries, as presented in Figure 1. It does not satisfactorily explain the intercalation dynamics of relatively flexible materials such as graphite, which show signs of high-order staging;[1,16] the scheme cannot account for the transitions from odd to even stages without a de-intercalation process.[17] However, LDHs do not manifest experimental evidence for stage orders higher than 2 at room temperature,[5–7,17] suggesting a Rüdorff pathway is possible for these types of materials.

The Daumas−Hérold[15] model is a more widely accepted scheme which explains the intercalation pathway of graphite.[2–4] The Daumas−Hérold model suggests that islands of intercalants are formed, called domains, as shown in Figure 1. If one domain is viewed in cross-section (indicated by dashed lines in Figure 1), it can be seen that a pattern similar to a Rüdorff model is encountered. The Daumas−Hérold model assumes that layered materials are flexible enough to deform around intercalant species. The energetic cost of host layer distortion causes two intercalants within the same interlayer to attract each other, while intercalants in adjacent layers are repelled.[2] Theoretically it has been shown that elastic interaction between intercalants is most likely the primary factor which causes the staging phenomena in materials such as graphite and transition-metal dichalcogenides.[3] Techniques such as dynamic high-resolution transmission electron microscopy have been used to visually detect intercalant islands in transition-metal dichalcogenides.[18] Some earlier theoretical studies by Safran and co-workers[2,19] used elastic properties of graphite intercalation compounds to predict a limiting temperature above which only stage-1 compounds exist,[19] called the transition temperature.[2] In this way, phase diagrams are produced which show that more flexible host compounds cause increased interaction between intercalant domains; as a result, layered compounds such as graphite have higher transition temperatures than more rigid materials such as clays.[3] The bending modulus of graphite sheets is obtained from experimental phonon dispersion relations which report a value of 9.93×10^{-20} J.[20] Although similar direct experimental results for the bending modulus of LDHs and smectite clays have not been reported, we have used molecular dynamics (MD) techniques to determine values of 8.3×10^{-19} J for LDHs[21] and 1.6×10^{-17} J for montmorillonite.[22] In addition, past studies have used a layer rigidity model to quantify transverse rigidity in layered solids such as graphite, vermiculite and LDHs.[23,24] These studies found that LDH layers are much more rigid than graphite, less rigid than vermiculite,[24] but of similar rigidity to metal dichalcogenides.[25] Intercalation of DNA was not found to change the simulated bending modulus of the Mg_2Al LDH sheets.[26]

(13) Greenwell, H. C.; Coveney, P. V. *Origins Life Evol. Biosphere* **2006**, *36*, 13–37.
(14) Rüdorff, W. *Z. Phys. Chem.* **1940**, *45*, 42.
(15) Daumas, N.; Hérold, A. *C. R. Seances Acad. Sci., Ser. C* **1969**, *268*, 373.
(16) Dahn, J. R. *Phys. Rev. B* **1991**, *44*, 9170–9177.
(17) Fogg, A.; Dunn, J.; O'Hare, D. *Chem. Mater.* **1998**, *10*, 356–360.
(18) McKelvy, M.; Sidorov, M.; Marie, A.; Sharma, R.; Glaunsinger, W. *Chem. Mater.* **1994**, *6*, 2233–2245.
(19) Safran, S. A. *Phys. Rev. Lett.* **1980**, *44*, 937–940.
(20) Zabel, H.; Magerl, A.; Rush, J. J. *Phys. Rev. B* **1983**, *27*, 3930–3933.
(21) Thyveetil, M.-A.; Coveney, P. V.; Suter, J. L.; Greenwell, H. C. *Chem. Mater.* **2007**, *19*, 5510–5523.
(22) Suter, J. L.; Coveney, P. V.; Greenwell, H. C.; Thyveetil, M.-A. *J. Phys. Chem. C* **2007**, *111*, 8248–8259.
(23) Solin, S. A.; Hines, D.; Yun, S. K.; Pinnavaia, T. J.; Thorpe, M. F. *J. Non-Cryst. Solids* **1995**, *182*, 212–220.
(24) Kim, H.; Jin, W.; Lee, S.; Zhou, P.; Pinnavaia, T. J.; Mahanti, S. D.; Solin, S. A. *Phys. Rev. Lett.* **1988**, *60*, 2168–2171.
(25) Solin, S. A. *Annu. Rev. Mater. Sci.* **1997**, *27*, 89–115.
(26) Thyveetil, M.-A.; Coveney, P. V.; Greenwell, H. C.; Suter, J. L. *J. Am. Chem. Soc.* **2008**, *130*, 4742–4756.

Numerous anion-exchange reactions of dicarboxylate ions with LDHs initially intercalated with chloride ions[17] exhibit second-order staging, as determined from time-resolved *in situ* energy-dispersive X-ray powder diffraction data.[17] Williams et al.[10,27−29] have also reported that intercalants such as phosphonate and succinate show second-order staging during anion-exchange experiments. The authors found that the occurrence of stage-2 phases also depends on temperature; a transition temperature of 60 °C appears to exist for phosphonate anions, above which stage-2 phases do not exist.

In previous studies,[21,26] we have used large-scale molecular dynamics to calculate elastic properties of the LDH $[Mg_2Al(OH)_6]Cl\cdot nH_2O$ which showed that the LDH layers are flexible enough to exhibit thermal undulations. Our simulations demonstrate that the LDH layers can deform around DNA; this effect was accentuated as the system became increasingly dehydrated.[21] The results indicate that, in a mixed interlayer region which has a large discrepancy in size between intercalant ions, deformation of host LDH layers can occur, providing a mechanism for the formation of staged intermediates through a Daumas−Hérold route. Deformation of LDH layers around intercalants has also been observed experimentally for the bulky $SmW_{10}O_{36}^{9-}$ ion intercalated into Mg,Al LDHs.[30] This material has been shown to undergo a transition from stage-1 at temperatures of 290 K to stage-2 and even stage-3 compounds at 28 K;[30] these results appear broadly consistent with Safran's predictions for Daumas−Hérold pathways.[19]

Experimental studies have shown that DNA strands, of less than 100 base pairs, can be ion-exchanged for nitrate ions in LDHs with very high efficiency.[31,32] However, it is surprising that such bulky anions as DNA are able to efficiently ion-exchange at all with relatively small species such as nitrate; as the interlayer space is very restrictive, the findings suggest that staged structures may be formed. In the past, it has been found necessary to pretreat LDHs with intermediate-sized species, such as terephthalate, in order to pre-expand the interlayer so as to accommodate bulky anionic species.[33] In this paper, we investigate three possible structures which could form during the intercalation of DNA into $[M_2Al(OH)_6]Cl$ LDHs through anion exchange with chloride ions. Though previous experimental work uses nitrate, chloride is also a readily exchangeable anion in LDHs. The choice of nitrate in the experimental work is invariably based on the facile preparation of the host LDH structure from the extremely soluble metal nitrate salts under basic conditions. In previous studies, analysis of infrared spectra and circular dichroism has provided strong evidence for full anion exchange of DNA for nitrate.[32,34] To study intercalation mechanisms, we have only partially exchanged the chloride anions for DNA anions. The structures represent a Daumas−Hérold model, a Rüdorff model, and a stage-1 model which has the same number of DNA strands as the two previous models but a sparser distribution of DNA. The purpose of the simulations is to identify structural, energetic, and dynamic diffusion properties in order to ascertain which of these configurations is more favorable as a potential model for intercalation.

2. Methods

2.1. Simulations. Three models were used to simulate the different possible configurations adopted by intercalated DNA strands in LDH. The original structural formula of the LDH we use, without intercalated DNA, is $[Mg_2Al(OH)_6]Cl\cdot 2H_2O$. This structure was also used in our previous studies,[21,26] but in the present work four layers per supercell were simulated. In order to maintain overall charge neutrality, sufficient chloride ions were removed from each gallery which contained DNA; each phosphate group in the DNA carried unit negative charge. The first model represents a Daumas−Hérold configuration, which places DNA in every layer, but offset relative to one another, to form DNA island domains, as shown in Figure 2b. The second represents a stage-2 Rüdorff model which has every other layer of LDH galleries filled with DNA (Figure 2c). The third model consists of DNA stacked in a stage-1 arrangement with all galleries filled and DNA strands stacked directly on top of each other in adjacent layers (Figure 2d). Throughout the simulation, the DNA strands were at least 15 Å from the edge of the simulation cell in the *ab* crystallographic plane to prevent self-interaction.

We have previously calculated the hydration curve for the LDH−DNA system and concluded that between 9 and 11 water molecules per $[Mg_2Al(OH)_6]$ unit are needed to reproduce experimental basal spacings,[21] which are between 21.1 and 23.9 Å for Mg_2Al−DNA systems.[31,35] In all three models in the present study, 9 water molecules per unit $[Mg_2Al(OH)_6]$ formula reside in each interlayer region, which corresponds to 9216 water molecules per interlayer. All three models contained 138 016 atoms for ease of quantitative comparisons. We have shown that small LDH models suffer from finite size effects which cause the suppression of thermal undulations; these thermal undulations are unrelated to periodic effects created upon replication of the unit cell.[21] The largest wavelength of thermal undulations is found to be 40 Å; the simulation cells used in this study were more than twice this distance. The DNA molecule studied was generated as an idealized structure from the Leap module of Amber[36] and is a B-form linear duplex dodecamer strand (Figure 2a). The sequence of the DNA strand is $d(CTTTTGCAAAAG)_2$; we use it in order to facilitate a direct comparison with previous simulations.[26,37,38]

The potential energy of the system is parametrized using a hybrid approach that combines the ClayFF,[39] which is a force field for the simulation of minerals such as LDHs, and the Amber ff99 force field[36] used to simulate DNA.[40,41] ClayFF produces good agreement with experiment for LDHs in terms of lattice parameters, water diffusion coefficients, and far-infrared spectra,[42−45] while the Amber force field is well established for the simulation of nucleic

(27) Williams, G. R.; Norquist, A. J.; O'Hare, D. *Chem. Commun.* **2003**, 1816–1817.
(28) Williams, G. R.; O'Hare, D. *J. Mater. Chem.* **2006**, *16*, 3065–3074.
(29) Williams, G. R.; Fogg, A. M.; Sloan, J.; Taviot-Guého, C.; O'Hare, D. *Dalton Trans.* **2007**, 3499–3506.
(30) Park, T.-R.; Park, T. Y.; Kim, H.; Min, P. *J. Phys.: Condens. Matter* **2002**, *14*, 11687–11700.
(31) Choy, J.-H.; Kwak, S.-Y.; Jeong, Y.-J.; Park, J.-S. *Angew. Chem.* **2000**, *39*, 4041–4045.
(32) Choy, J.-H.; Kwak, S.-Y.; Park, J.-S.; Jeong, Y.-J.; Portier, J. *J. Am. Chem. Soc.* **1999**, *121*, 1399–1400.
(33) Drezdzon, M. A. *Inorg. Chem.* **1988**, *27*, 4628–4632.
(34) Oh, J.-M.; Kwak, S.-Y.; Choy, J.-H. *J. Phys. Chem. Solids* **2006**, *67*, 1028–1031.
(35) Desigaux, L.; Belkacem, M. B.; Richard, P.; Cellier, J.; Leone, P.; Cario, L.; Leroux, F.; Taviot-Gueho, C.; Pitard, B. *Nano Lett.* **2006**, *6*, 199–204.
(36) Kollman, P. A.; Wang, J.; Cieplak, P. *J. Comput. Chem.* **2000**, *21*, 1049–1074.
(37) Jha, S.; Coveney, P. V.; Laughton, C. A. *J. Comput. Chem.* **2005**, *26*, 1617–1627.
(38) Harris, S. A.; Gavathiotis, E.; Searle, M. S.; Orozco, M.; Laughton, C. A. *J. Am. Chem. Soc.* **2001**, *123*, 12658–12663.
(39) Cygan, R. T.; Liang, J.-J.; Kalinichev, A. G. *J. Phys. Chem. B* **2004**, *108*, 1255–1266.
(40) Young, M. A.; Jayaram, B.; Beveridge, D. L. *J. Am. Chem. Soc.* **1997**, *119*, 59–69.
(41) Hobza, P.; Kabelac, M.; Sponer, J.; Vondrasek, J.; Mejzlík, P. *J. Comput. Chem.* **1997**, *18*, 1136–1150.
(42) Wang, J.; Kalinichev, A. G.; Kirkpatrick, R. J.; Hou, X. *Chem. Mater.* **2001**, *13*, 145–150.
(43) Kalinichev, A. G.; Kirkpatrick, R. J. *Chem. Mater.* **2002**, *14*, 3539–3549.

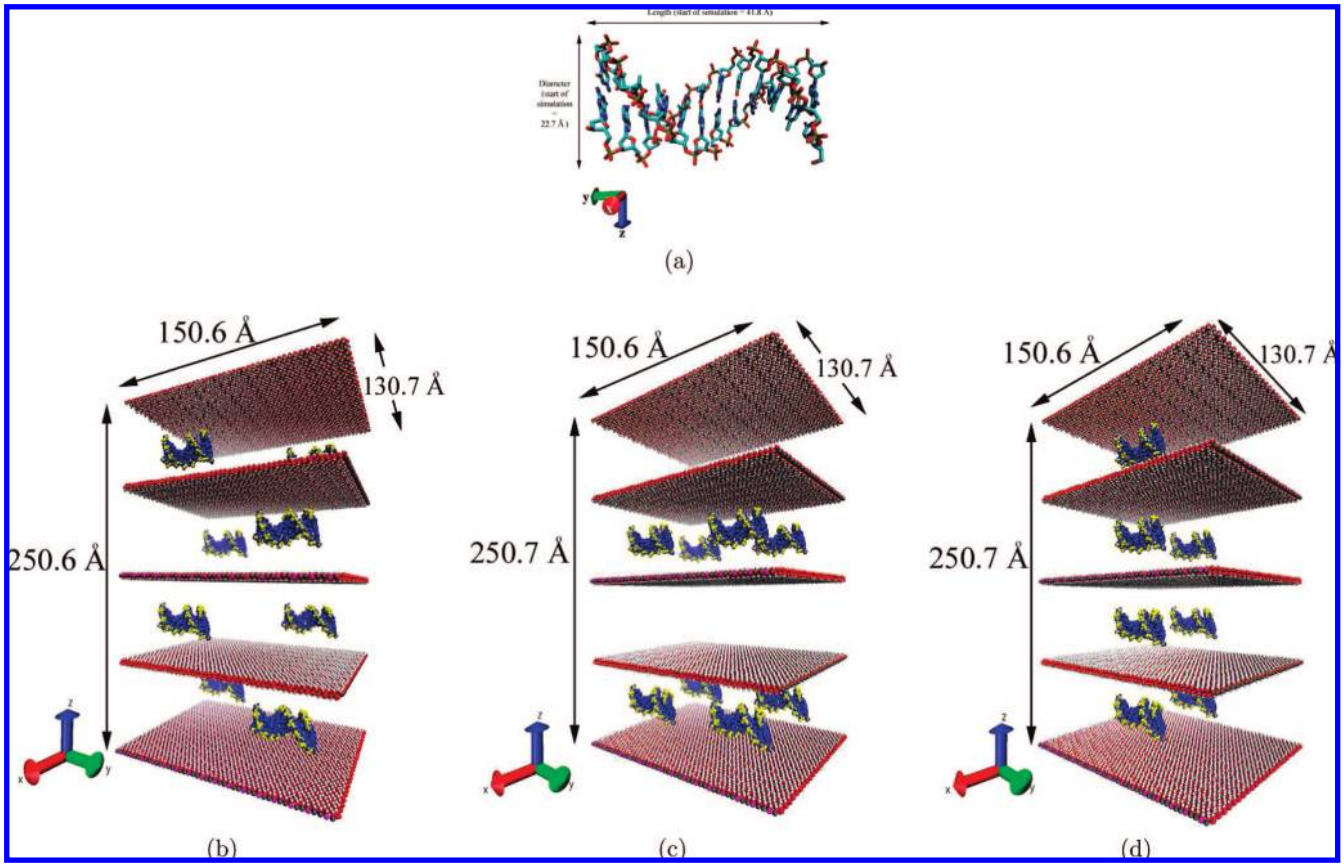

Figure 2. Starting structures for our molecular dynamics simulations. (a) DNA with carbon, nitrogen, oxygen, and phosphate atoms represented as cyan, blue, red, and green, respectively, with hydrogen atoms not displayed. (b) System **I** (Daumas−Hérold), (c) system **II** (Rüdorff), and (d) system **III** (stage-1). The major axes of the DNA strands lie along the *y*-direction. For clarity, water molecules and chloride ions are not displayed. Magnesium, aluminum, oxygen, and hydrogen atoms within the LDH are represented as gray, pink, red, and white spheres, respectively; the atoms within the DNA phosphate backbone are shown as yellow spheres; and all other atoms within the DNA strands are represented as blue spheres. The total number of atoms in each model, panels b−d, is identical at 138 016 atoms.

acids—it is known to reproduce the structure and dynamics of nucleic acid moieties well, including Watson−Crick base pairing.[40,41] DNA and LDH interact via nonbonded (electrostatic and van der Waals) interactions only. The missing Lennard-Jones intermolecular potential parameters are supplemented using Lorentz−Berthelot mixing rules. These methods suffice for systems dominated by electrostatics,[46−48] as shown in our earlier study.[26] Water molecules are described using the flexible single point charge model.[49]

The systems were simulated using the large-scale atomistic/molecular massively parallel simulator (LAMMPS),[50] a highly scalable, parallel molecular dynamics program which can be run on a variety of computer architectures. We energy-minimized the systems before carrying out the MD simulations, using techniques discussed in our previous studies.[21,26] The production runs for systems **I**, **II**, and **III** were performed for 4.78, 4.60, and 4.36 ns, respectively, to capture any diffusion data for the DNA molecules. The simulations were carried out at 300 K and 1 atm, using a Nosé-Hoover thermostat/barostat to regulate the temperature and pressure of each simulation. The post-processing analysis of DNA was performed using the 3DNA software analysis tool.[26,51] To quantify the overall change in the DNA structures, the root-mean-square displacement (rmsd) was calculated by removing translational and rotational degrees of freedom through a least-squares fit, followed by rotation to the original reference frame of the molecule. The rmsd is computed from the following equation:

$$r_{\mathrm{rmsd}}(\mathbf{r}, \mathbf{r}_0) = \sqrt{\frac{1}{N}\sum_{i=1}^{N}(\mathbf{r}_i - \mathbf{r}_{i,0})^2} \qquad (1)$$

where $\mathbf{r}$ is the current position of atom i, and $\mathbf{r}_{i,0}$ is its initial position. The initial position of DNA was taken from the initial idealized structure built using the Amber module Leap.

Principal component analysis (PCA) was used to describe the main changes in DNA structure with time, in order to reduce the dimensionality of the MD trajectory, hence identifying the dominant collective modes of motion of the DNA.[37,52−54] In order to compare the mobility of the DNA strands, the diffusion coefficient of each molecule was also calculated. The diffusion coefficient is calculated from the slope of the mean-square displacement (MSD, δr^2) vs time graph. The MSD was computed from the center of mass of each DNA duplex strand in order to include only translational

(44) Wang, J.; Kalinichev, A. G.; Amonette, J. E.; Kirkpatrick, R. J. *Am. Mineral.* **2003**, *88*, 398–409.
(45) Wang, J.; Kalinichev, A. G.; Kirkpatrick, R. J. *Geochim. Cosmochim. Acta* **2006**, *70*, 562–582.
(46) Duffy, D. M.; Harding, J. H. *Langmuir* **2004**, *20*, 7630–7636.
(47) Cormack, A. N.; Lewis, R. J.; Goldstein, A. H. *J. Phys. Chem. B* **2004**, *108*, 20408–20418.
(48) Harding, J. H.; Duffy, D. M. *J. Mater. Chem.* **2006**, *16*, 1105–1112.
(49) Berendsen, H. J. C.; Postma, J. P. M.; von Gunsteren, W. F.; Hermans, J. *Intermolecular Forces*, 1st ed.; Reidel Publishing Co.: Dordrecht, The Netherlands, 1981.
(50) Plimpton, S. *J. Comput. Phys.* **1995**, *117*, 1–19.
(51) Lu, X.-J.; Olson, W. K. *Nucleic Acids Res.* **2003**, *31*, 5108–5121.
(52) Hess, B. *Phys. Rev. E* **2000**, *62*, 8438–8448.
(53) de Groot, B. L.; Daura, X.; Mark, A. E.; Grubmuller, H. *J. Mol. Biol.* **2001**, *309*, 299–313.
(54) Amadei, A.; Linssen, A. B. M.; Berendsen, H. J. C. *Proteins* **1993**, *17*, 412–425.

motion in the calculation. The graph is constructed using multiple origins in order to improve the statistics of the calculation. As the DNA molecules are constrained to move within the interlayer planes, the diffusive motion is confined to the *xy*-plane. Therefore, we compute values for the two-dimensional diffusion coefficient, which is given by $4D_{xy} = (\mathrm{d}/\mathrm{d}t)\delta r^2$, where $\delta r^2 = (\delta x^2 + \delta y^2)/2$. The δr^2 vs time plot exhibits a linear region of slope D, and we find the error on the least-squares fit to estimate the error of the diffusion coefficient. We make structural comparisons with experiment by computing XRD spectra from our simulations using the Diffraction-Crystal module of Cerius2.[55] The calculations included Debye−Scherrer instrumental broadening using the pseudo-Voigt method which is a weighted sum of Gaussian and Lorentzian functions.[55] Thermal atomic vibrations were also included, as well as line broadening effects due to experimentally determined crystallite sizes of 100 nm × 100 nm × 10 nm.[56] The powder X-ray diffraction (PXRD) patterns simulate those obtained with Cu Kα radiation (λ = 1.5418 Å). We also included preferred orientation effects, common in anisotropic crystals, such as LDH, when pressed onto an XRD slide.

Simulations were performed on the NGS-2 nodes of the UK's National Grid Service (www.ngs.ac.uk), specifically sites at Leeds and the Rutherford Appleton Laboratory, as well as the TeraGrid machine Bigben at Pittsburgh Supercomputing Center (www.psc.edu). Submission of jobs was facilitated by the Application Hosting Environment (AHE, www.omii.ac.uk).[57] Visualization was also needed in order to qualitatively understand the evolution of the simulations. AtomEye[58] and VMD[59] were used as they efficiently render large numbers of atoms. We made use of switched optical networking in order to transfer data generated in this study by utilizing the JANET lightpath network (www.ja.net) which acts as a dedicated, high-speed link within the UK and connects to similar network infrastructures across Europe and the USA.[60]

2.2. Analysis of Peristaltic Modes. LDH sheets were shown in our previous study to be flexible enough to distort around bulky intercalant species such as DNA.[26] The change in basal spacing can be used to quantify peristaltic modes which appear within the system, and thus help to understand the mechanism of DNA diffusion between LDH sheets during intercalation. We previously used the Helfrich free energy to describe the bending energy of clay sheets, which allowed us to compare bending moduli.[21,22] This continuum method can also be applied to the thickness fluctuations of the basal spacing to identify peristaltic modes.[61,62] The amplitude of the fluctuations, denoted by $t(x,y,n)$, is defined as $t(x,y,n) = (b(x,y,n) - b_{0,n})/2$, where $b(x,y,n)$ is the basal spacing at position (x,y) within the nth interlayer and $b_{0,n}$ is the mean basal spacing of the nth interlayer. The spectral intensity of the peristaltic modes with amplitude $t(x,y,n)$ can be described as a function of the wave vector q by[61]

$$\langle t(q)^2 \rangle = \begin{cases} \dfrac{kT}{A(k_{\mathrm{d}}q^4 + \gamma q^2 + k_{\mathrm{e}})} & \text{for } q < q_0 \\ \dfrac{kT}{A\gamma q^2} & \text{for } q > q_0 \end{cases}$$

where k_{d} represents the bending modulus of the peristaltic modes, k_{e} is a harmonic constant which accounts for the restorative force for the basal spacing to return to its equilibrium value, $b_{0,n}$, γ is the surface tension, k is Boltzmann's constant, and T is the temperature. q_0 corresponds to the correlation wavevector which is related to the correlation wavelength, $\lambda_0 = 2\pi/q_0$.[62] At length scales smaller than λ_0, this describes peristaltic modes; above the correlation length, neighboring LDH layers interact and exhibit q^{-2} behavior.[21,22]

The fluctuation in basal spacing $t(x,y,n)$ is found from the difference in height of two adjacent LDH layers. The surface of each LDH layer is described using a rectangular mesh, and the z-coordinates of LDH atoms are averaged within each segment to find the height of that portion of the nth surface at $z(x,y,n)$. The amplitude of the thickness fluctuations, $t(x,y,n)$, is found by subtracting each $z(x,y,n)$ element in two adjacent layers. The spectral intensity is calculated by performing a two-dimensional discrete Fourier transform on $t(x,y,n)$. This decomposes the basal spacing into a continuous spectrum of wavevectors, q, of magnitude $2\pi/\lambda$, where λ is the wavelength of the peristaltic modes. If peristaltic modes exist within the system, the spectral intensity will vary as q^{-4} at wavelengths smaller than the correlation length but greater than surface protrusions.

3. Results

In this section we present our main results concerning the properties of the LDH−DNA systems in different stacking arrangements. We quantify these differences energetically and by analyzing the structure, as well as the simulated PXRD patterns and diffusion data. Structural analysis of DNA is carried out by calculation of the rmsd with respect to the initial structures and the number of intact Watson−Crick hydrogen bonds. The diffusion properties of DNA molecules in the different stacking arrangements provides insight into possible mechanisms for the intercalation of DNA, and other large molecules, within the nanoscopic galleries of LDHs.

3.1. Structure of the LDH−DNA System. Visualization of the atomic trajectories (shown in Figure 3) illustrates the flexibility of the LDH sheets. Visualization shows that the layers in system **I** form Daumas−Hérold structures when DNA is stacked in this arrangement. The Rüdorff model in system **II** also shows evidence of layer bending. Systems **I** and **II** show layer deformation around DNA because neighboring interlayers directly above and below are unoccupied by DNA molecules; instead there are much smaller chloride ions present in these regions. However, the LDH layers in system **III** remain relatively flat as a result of conflicting forces between adjacent layers hosting DNA molecules. It can be seen that, in some instances, Mg^{2+} cations diffuse out of the LDH layers into the interlayer region; around 2% of all Mg^{2+} in the LDH layers exhibit this behavior. While this phenomenon may be a physical effect, it could also be caused by deficiencies in the ClayFF force field.[21,26]

In Figure 4, we present calculated PXRD patterns and compare them with experimental data. The experimental diffractograms were from Desigaux et al.,[35] who intercalated a wide variety of DNA molecules between 100 and 1000 base pairs (bps) long using the co-intercalation method which forms LDH around DNA strands, and from Choy et al.,[32] who used anion exchange to intercalate a narrower range of DNA strands, between 500 and 1000 bps long. The difference in experimental PXRD data, shown in Figure 4, highlights the different formation mechanisms that may arise depending on preparation technique. The experimental XRD patterns show that the systems are quite disordered: there are broad "saw-tooth" peaks indicative of turbostratic disorder and an inferred wide range of basal spacings about a mean value.[32,35] Desigaux's XRD

(55) Accelrys Software Inc., www.accelrys.com.
(56) Kwak, S.-Y.; Park, J.-S.; Jeong, Y.-J.; Choy, J.-H. *Solid State Ionics* **2002**, *151*, 229–234.
(57) Coveney, P. V.; Saksena, R. S.; Zasada, S. J.; McKeown, M.; Pickles, S. *Comput. Phys. Commun.* **2007**, *176*, 406–418.
(58) Li, J. *Modell. Simul. Mater. Sci. Eng.* **2003**, *11*, 173–177.
(59) Humphrey, W.; Dalke, A.; Schulten, K. *J. Mol. Graphics* **1996**, *14*, 33–38.
(60) Coveney, P. V.; Giupponi, G.; Jha, S.; Manos, S.; Suter, J. L.; Thyveetil, M.-A.; Zasada, S. J. *Fut. Gen. Comp. Sys.* **2008**, in press.
(61) Marrink, S. S.; Mark, A. *J. Phys. Chem. B* **2001**, *105*, 6122–6127.
(62) Lindahl, E.; Edholm, O. *Biophys. J.* **2000**, *79*, 426–433.

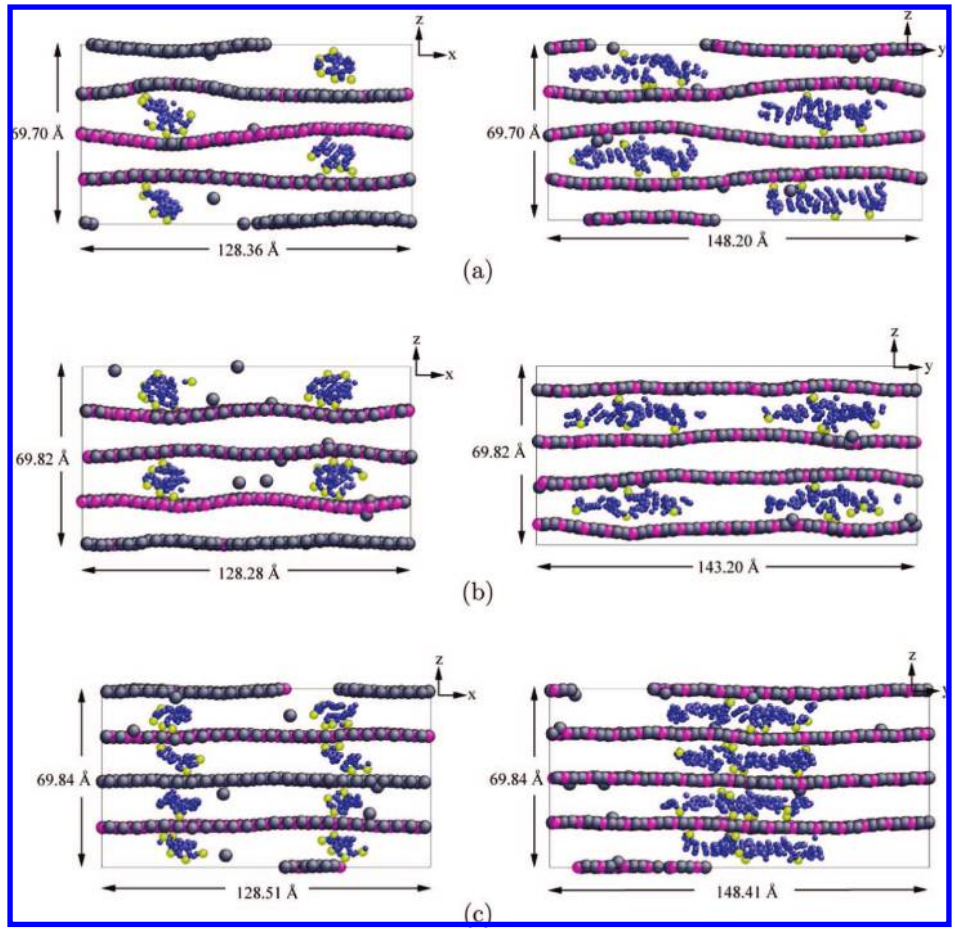

Figure 3. Two-dimensional slices in the *xz* and *yx* planes of DNA duplices within partially ion-exchanged $[Mg_2Al(OH)_6]Cl\cdot 9H_2O$ for (a) system **I** (Daumas−Hérold configuration), (b) system **II** (Rüdorff configuration), and (c) system **III** (stage-1 configuration). The figures were produced using AtomEye[58] and taken as snapshots of the systems after 4.0 ns of production simulation. The color coding of aluminum, magnesium, carbon, nitrogen, and phosphorus atoms is the same as Figure 2; oxygen, hydrogen, and chloride ions have not been displayed for clarity.

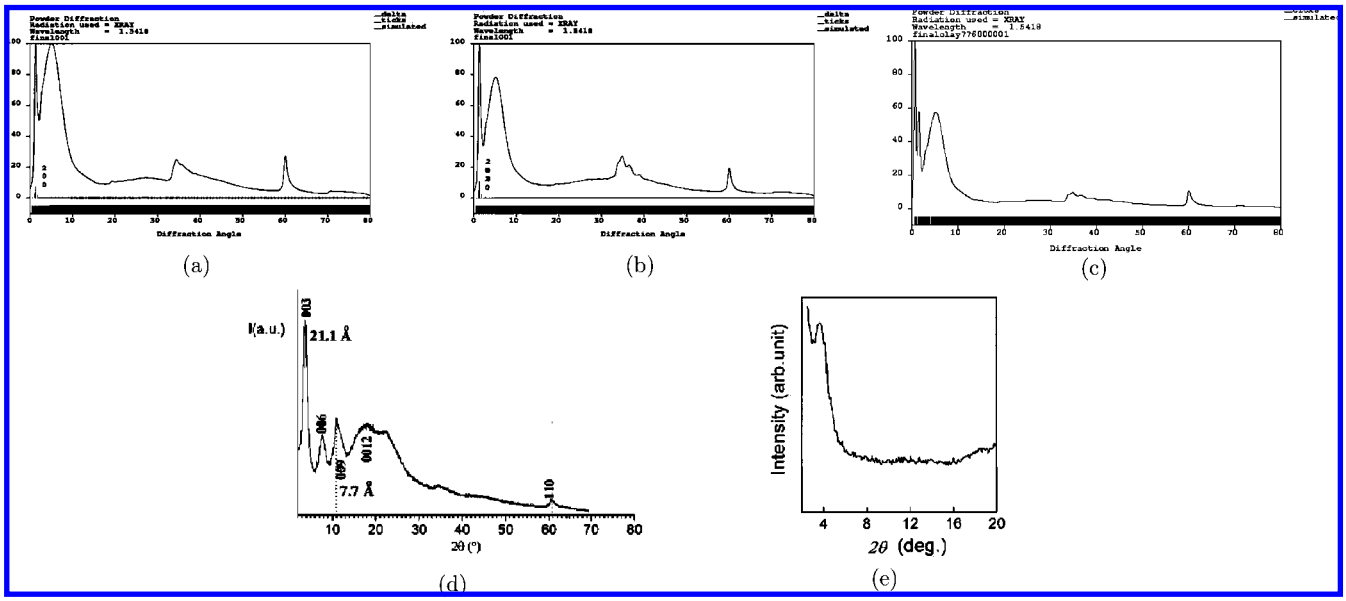

Figure 4. Simulated powder X-ray diffractogams for (a) system **I** (Daumas−Hérold), (b) system **II** (Rüdorff), and (c) system **III** (stage-1), compared with experimental XRD data produced by (d) Desigaux et al.[35] and (e) Choy et al.[32] The simulated XRD patterns were produced using the final snapshot of each system. The LDH−DNA systems manifest disorder through the broad peaks which are present in the experimental and simulated diffractograms.

patterns show peaks which correspond to the existence of basal spacings caused by nitrate anions and DNA molecules within the interlayer region, suggesting that samples can be mixed and contain both intercalated species.[35] The simulated XRD patterns

Table 1. Properties of Systems **I**, **II**, and **III** Averaged over the Production Phase of Simulation[a]

		average simulation cell dimensions (Å)			
system	potential energy ($\times 10^6$ kcal/mol)	L_x	L_y	L_z	maximum basal spacing (Å)
I	-3.8637 ± 0.0004	128.4 ± 0.04	148.3 ± 0.05	69.7 ± 0.06	22.8 ± 0.3
II	-3.8640 ± 0.0004	128.3 ± 0.05	148.2 ± 0.05	69.8 ± 0.06	20.2 ± 0.3
III	-3.8629 ± 0.0004	128.5 ± 0.04	148.4 ± 0.05	69.8 ± 0.06	19.5 ± 0.3

[a] Errors are from the standard deviation. The basal spacings of systems **I** and **II** vary substantially over the orthogonal dimensions of the models; the maximum basal spacing is given for comparison with system **III**.

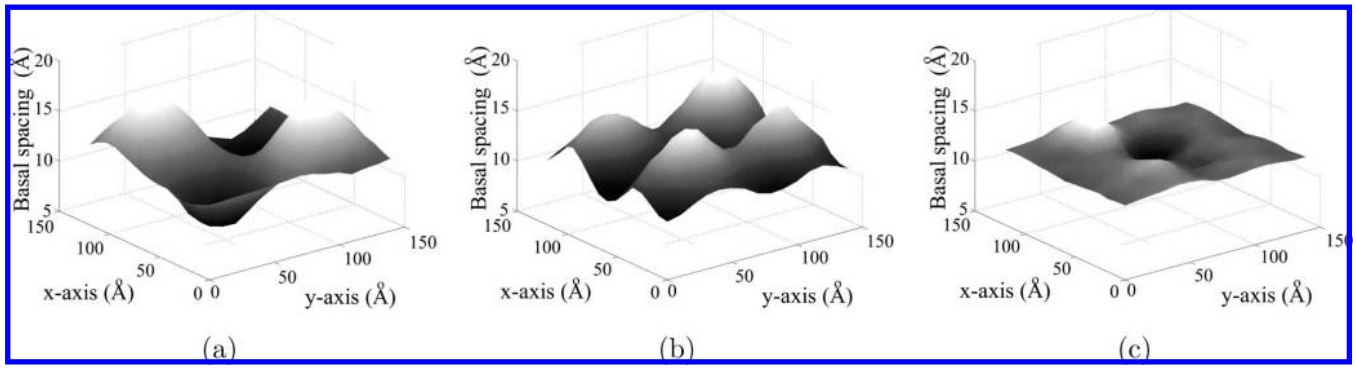

Figure 5. Three-dimensional plots showing the change in basal spacing of the LDH around intercalated DNA. The images were created by averaging the distance between adjacent layers over 4.0 ns for (a) system **I**, which has maximum and minimum basal spacings of 22.8 and 12.8 Å, respectively; (b) system **II**, which has maxima and minima of 20.2 and 12.9 Å, respectively; and (c) system **III**, which has maxima and minima at 19.5 and 15.6 Å, respectively. Regions with the largest basal spacings in systems **I** and **II** coincide with locations where DNA molecules reside. In system **III**, DNA strands are stacked directly on top of each other.

of all systems reproduce the broad peak, seen in the experimental diffractograms. The forms of all the simulated diffractograms are very similar, the main differences lying in the broad peaks at a diffraction angle around $2\theta = 5°$, which has greatest intensity in system **I**. Overall, the diffractograms for all the simulated systems are in closer agreement with the experimental results of Choy et al.,[32] shown in Figure 4e, than those of Desigaux et al.[35]

Table 1 compares the potential energies of the systems, as well as the simulation cell dimensions. Due to the deformation of the LDH sheets, shown in Figure 3, around DNA, systems **I** and **II** exhibit a significant distribution of basal spacings. Previous studies have referred to the region of enlarged basal spacing around DNA molecules as the "catchment area".[63] Therefore, we report the maximum basal spacing and its standard deviation averaged over the production phase of the simulation. Analysis of the maximum basal spacing shows that the largest separation between LDH layers occurs in system **I**. Figure 5 shows plots of the average change in basal spacing for one layer in each system and confirms that the largest deformations are around DNA in both systems **I** and **II**. Table 1 reports that the length of the simulation cell in the *z*-direction is smallest in system **I**, despite a large deformation around DNA strands, which indicates that the alternating expansion and contraction seen in a Daumas−Hérold model cause the unit cell to compress overall in the *z*-direction. The potential energies give an indication of the relative mechanical stability of each configuration. The potential energies are very similar in all models: systems **I** and **II** have similar energies which are slightly lower than that of system **III**, with its stage-1 stacking configuration. As the potential energies of systems **I** and **II** are within error bars of each other with neither being energetically favored, it is possible that one, or both, may be metastable states.

The fact that higher order staging is not seen in LDHs at room temperature may be due to layer flexibility and the hydration state of the host material. Transition-metal dichalcogenides, such as titanium sulfide intercalated with silver,[64] have similar layer flexibility and also generally show stage-2 structures.[18,64] Higher order stages are associated with more flexible materials, such as graphite; LDHs may not be flexible enough to form stages higher than 2 under ambient conditions.

3.2. Peristaltic Modes of Motion. Spectral analysis of the basal spacings shows that each of the models has distinctive behavior. The results are decomposed into *x* and *y* directions; DNA duplices are orientated with longest axes along the *y* axis, as shown in Figure 6. Peristaltic modes within a system are identified by a q^{-4} dependence when plotting spectral intensity vs wave vector. The Daumas−Hérold and stage-1 models most clearly show q^{-4} behavior compared to the Rüdorff model, in both the *x* and *y* directions, indicating that peristaltic modes are more prevalent in these systems. The data points in the *y* direction in the Rüdorff model have a better fit to q^{-4} behavior compared to those along *x*: peristaltic modes are more clearly evident in the direction in which DNA strands are principally aligned. This in turn suggests that DNA strands are more likely to propagate along the *y* axis compared to *x*. The Supporting Information contains animations of the change in basal spacing with time; from these it is apparent that the islands of intercalant show evidence of an effective attraction between islands within the same interlayer, although longer simulations would need to be run in order to confirm that these islands do eventually merge.

The bending modulus of the peristaltic modes in the Rüdorff system is 1.04×10^{-19} J in the *x* direction and 3.77×10^{-21} J in the *y* direction. This suggests that there is greater flexibility in the structure supporting peristaltic modes in the *y* direction compared to the *x* direction. In contrast, the bending moduli of

(63) Thorpe, M. F. *Phys. Rev. B* **1989**, *39*, 10370–10372.

(64) Kaluarachchi, D.; Frindt, R. F. *Phys. Rev. B* **1983**, *28*, 3663–3665.

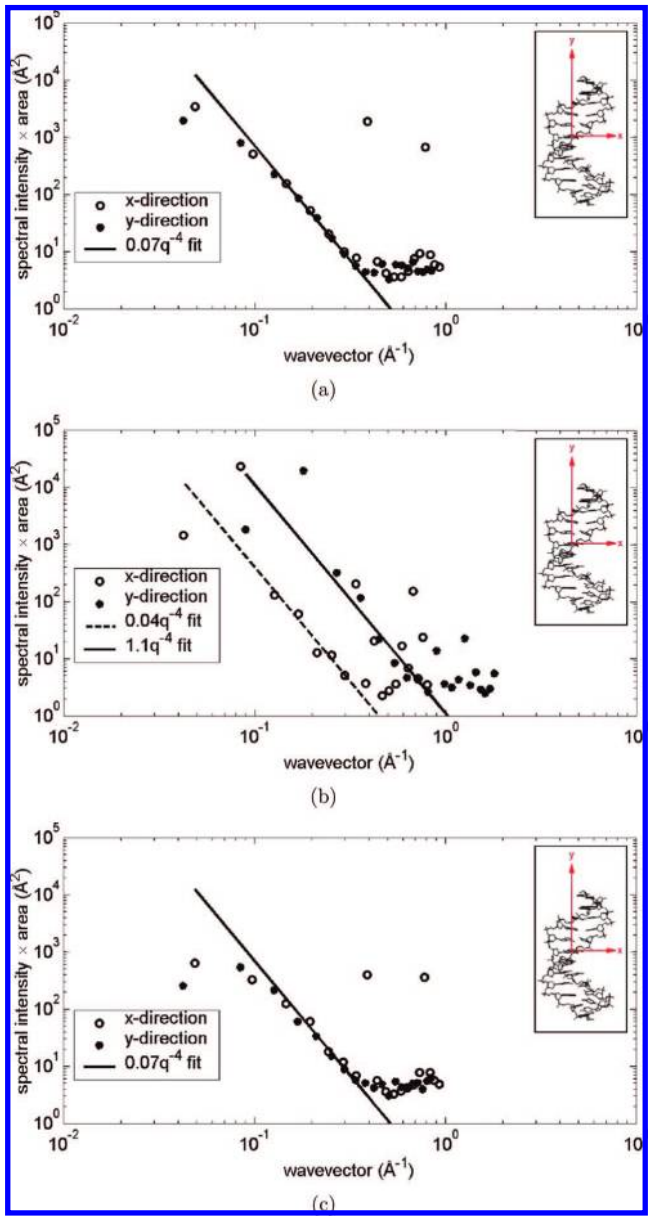

Figure 6. Spectral intensity analysis of the thickness variation of the basal spacing for (a) system **I** (Daumas−Hérold), (b) system **II** (Rüdorff), and (c) system **III** (stage-1). The presence of peristaltic modes of motion is identified by a q^{-4} behavior in the graphs, which is most clearly seen in systems **I** and **III**. However, the peristaltic modes are damped at shorter wavelengths in system **III** compared to system **I**. In both systems **I** and **III**, anomalous behavior is seen at wavelengths of ∼16.0 and ∼8.0 Å. The original unit cell used to create the models was 16.3 Å in the *x* dimension; these points are due to artifacts created upon replication of the unit cell.[21,22] The points representing the *y* direction of system **II** more closely follow q^{-4} behavior compared to those in the *x* direction.

the peristaltic modes in systems **I** and **III** are 5.92×10^{-20} J in both directions. System **III** also shows peristaltic behavior, even though there is relatively little deformation in LDH sheets around DNA compared to systems **I** and **II**. At lower wave vectors, the spectral intensity behavior of systems **I** and **III** diverges from q^{-4} due to interaction with neighboring LDH layers, being replaced by a q^{-2} behavior; the wave vector at which the behavior transitions from q^{-4} to q^{-2} is called the correlation length, as discussed in section 2.2. The correlation length in the stage-1 structures is approximately 49.4 Å, while the Daumas−Hérold model diverges significantly from q^{-4} behavior when the wavelength of the peristaltic modes reaches the simulation box dimensions.

Table 2. Structural Properties of DNA for the Three Different Models, Averaged over 4.0 ns[a]

system	DNA diameter (Å)	% of intact Watson−Crick hydrogen bonds	rmsd (Å)
I	15.4 ± 0.6	25 ± 8	3.5 ± 0.2
II	15.0 ± 0.6	17 ± 8	3.2 ± 0.2
III	12.4 ± 0.6	0 ± 0	2.5 ± 0.1
DNA in water	22.0 ± 1.2	78.1 ± 3	7.1 ± 0.2

[a] Error bars are calculated from the standard deviation of the data. Twelve-base-pair DNA duplex strands have been deformed from their initial structure generated from the Amber Leap module. Comparing the root-mean-square deviation (RMSD) from the initial structures, DNA diameter, and Watson−Crick hydrogen bonds, it can be seen that DNA strands are least deformed in the Daumas−Hérold configuration. Also included are the results for a linear 32-bp strand of DNA in bulk water, found from our previous study.[26]

3.3. Properties of Intercalated DNA. Within LDHs, the configuration DNA assumes is that of a more or less deformed double helix.[26] The deviation of DNA from its configuration in bulk water within these LDHs provides some indication as to the preferential stacking of DNA molecules during intercalation. Table 2 compares the average structural properties of the DNA duplex in each system. We have previously compared the structure of intercalated DNA with that of DNA in bulk water.[26] The strong electrostatic forces between the LDH sheets and DNA cause the intercalated molecules to be significantly constrained compared to DNA in bulk water.

Table 2 compares structural properties of the LDH-inter calated DNA strands with those of DNA in bulk water. The average diameter represents the size of the DNA in its radial direction. Compared to the other stacking arrangements, the Daumas−Hérold model is largest. The average rmsd of the DNA molecules, calculated relative to the initial model DNA structure in bulk water, is lowest for system **I**. System **I** also contains the largest number of intact Watson−Crick hydrogen bonds. However, compared to DNA in bulk water, Table 2 shows that base pairing becomes disrupted in all three models. In bulk water, we find that the average percentage of intact base pairs is around 80%;[26] we have also previously shown that intercalated DNA has varying numbers of hydrogen-bonded base pairs, depending on the number of co-intercalated water molecules.[26] Although all models in our present study have the same number of intercalated water molecules, DNA duplices are least distorted in the Daumas−Hérold structure. The radial distribution function (RDF) plots of Figure 7 show that, because DNA strands are less compressed in system **I** than in system **III**, fewer phosphate groups reside at the surface of the LDH sheets in system **I**. The phosphate groups in systems **I** and **II** are also more hydrated compared to system **III**, as shown by the relative intensities of the RDF peaks in Figure 7b.

PCA reveals the dominant contributions to the DNA dynamics. Once the direction of greatest motion has been established in the DNA molecules, the trajectory of this component can be superimposed, as shown in Figure 8. Figure 8 compares structural variations of the DNA strands which exhibit relatively large and small diffusion coefficients. Although the PCA results show little variation among all these models, superposition of a single DNA strand's atomic trajectory onto the first principal component eigenvector demonstrates that DNA molecules in the Daumas−Hérold model exhibit the greatest structural variation (this is confirmed by the larger variation in atomic projections onto the first eigenvector). Naïvely, one would

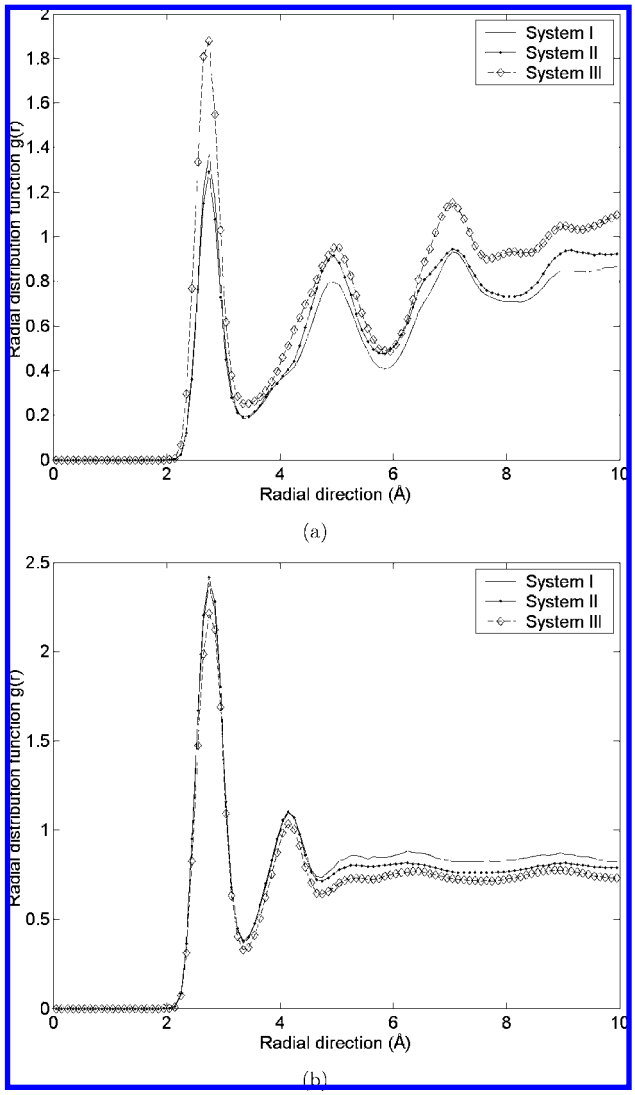

Figure 7. Radial distribution function between (a) phosphorus atoms in phosphate groups and hydrogen atoms in surface hydroxide groups and (b) phosphorus atoms in phosphate groups and hydrogen atoms in water. In system **III**, DNA strands are the most compressed, which in turn leads to more phosphate atoms residing at the surface of the LDH; this is confirmed by plot (a), which shows greater peak intensity at 2.75 Å. Plot (b) shows that phosphate groups in systems **I** and **II** have similar extents of DNA hydration, larger than that of DNA in system **III**.

expect eigenvectors of the atomic trajectories to be independent of each other, but the data displayed in the graphs in the bottom row of Figure 8 clearly contradict this, as the scatter plots form well-defined regions. This is because the diffusional motion of the DNA is heavily influenced by the LDH sheets.[26] The PCA plots in Figure 8 show that DNA molecules in systems **I** and **II** have larger amplitudes of motion compared to those in system **III**.

In our previous work we showed that hydration plays an important role in determining the system's basal spacing and the DNA conformations.[26] The present study demonstrates that the arrangement of multiple DNA strands also influences the basal spacing. We have also previously shown that, as the density of water within the galleries reaches that of bulk water, the LDH layers bend less because the hydration pressure becomes more dispersed, instead of being localized around each intercalated DNA moiety; therefore, the dynamics and diffusion properties of intercalated DNA will vary with hydration state. If staging in LDHs follows a Daumas−Hérold pathway, then, at greater levels of hydration, DNA−LDH systems in general may not show any significant staging, since there will be virtually no layer deformations around intercalated DNA.

3.4. DNA Diffusion. Although it is entirely possible that additional long-term diffusion processes not accessible on the time scale of our simulations take place in real systems, estimates of the short-term diffusion coefficients of the DNA can be calculated which provide an indication of the relative mobility of DNA in all three models. Figure 9 shows the behavior of the average MSD vs time for all DNA atoms in systems **I**−**III**. We find that individual strands of DNA have a wide variety of diffusion coefficients; Table 3 reports maximum, minimum, and average values for each system. The variety of diffusion coefficients seen in system **I** for individual DNA strands may be due to peristaltic behavior within the system which causes some DNA strands to diffuse faster than others. The table shows that, on average, the DNA molecules in system **II** exhibit slightly higher diffusivity within the interlayer plane than those in systems **I** and **III**. The largest diffusion coefficient is found to be $(2.8 \pm 0.01) \times 10^{-12}$ m^2 s^{-1} in both the Daumas−Hérold and Rüdorff models, approximately an order of magnitude less than the diffusion coefficient for intercalated water molecules, $\sim 1 \times 10^{-11}$ m^2 s^{-1}.[21,65,66] Unsurprisingly, diffusion of the intercalated DNA strands is smaller than that of DNA in bulk water; we find that diffusion of a 32-bp DNA strand in bulk water is $(5.3 \pm 0.8) \times 10^{-11}$ m^2 s^{-1}. Overall, the DNA diffusion coefficients for systems **I** and **III** are smaller than those for system **II**, but system **I** has the same range of values as system **II**.

The motion of DNA molecules is heavily dependent on the motion of the LDH sheets due to the dominating electrostatic interactions between phosphate groups and the LDH surface.[26] If all the atomic spatial trajectories of phosphorus atoms in phosphate groups are superimposed, it is apparent that the phosphate groups reside around discrete regions on the LDH surface. Figure 10 is an example of a phosphorus atom residing around multiple locations on the LDH surface. Calculation of the radial distribution function for phosphate groups and the different types of atoms in the LDH layers shows that phosphate groups preferentially cluster closer to aluminum than magnesium.[26] Figure 10 indicates that the negatively charged phosphate groups hop between these positively charged aluminum sites along the LDH surface.

It is instructive to compare these findings to those for cations intercalated within cationic clays, such as sodium ions within montmorillonite.[67] The self-diffusion coefficient of intercalated sodium ions within montmorillonite is reported from simulation to be between 1×10^{-11} and 1×10^{-10} m^2 s^{-1},[67] depending upon the hydration state of montmorillonite,[67,68] and water molecules within the same system have a diffusion coefficient between 1×10^{-10} and 1×10^{-9} m^2 s^{-1}.[67] The average diffusion coefficient found in this study for individual DNA strands is approximately an order of magnitude less than those found for cations within montmorillonite. However, DNA strands are much larger and more highly charged than simple

(65) Kagunya, W. W. *J. Phys. C* **1996**, *100*, 327–330.
(66) Marcelin, G.; Stockhausen, N. J.; Post, J. F. M.; Schutz, A. *J. Phys. C* **1989**, *93*, 4646–4650.
(67) Chang, F. R. C.; Skipper, N. T.; Sposito, G. *Langmuir* **1995**, *11*, 2734–2741.
(68) Boulet, P.; Coveney, P. V.; Stackhouse, S. *Chem. Phys. Lett.* **2004**, *389*, 261–267.

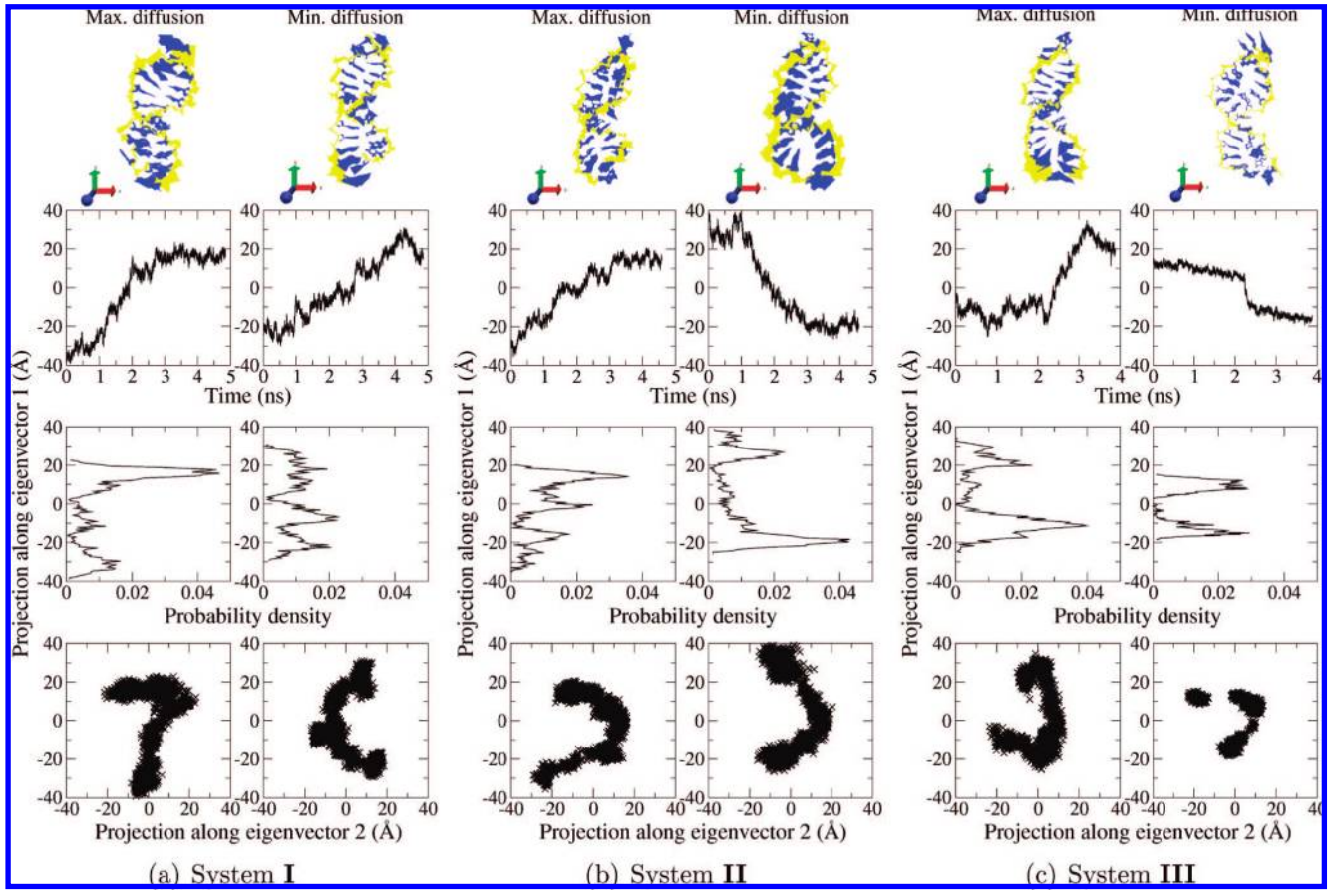

Figure 8. Comparison of principal component analysis for DNA molecules with the largest and smallest two-dimensional diffusion coefficients for (a) system **I**, (b) system **II**, and (c) system **III**. The uppermost row represents the superposition of all configurations obtained by projecting the motion of heavy atoms, P, C, O, and N onto the first eigenvector using PCA. The configurations are averaged over the production phase of the simulations, and the visualizations are viewed in the *xy* plane; the longitudinal axis of DNA lies parallel to the LDH sheets. Yellow represents the phosphate backbone, while blue includes the sugar groups and base pairs. The second row displays the motion of heavy atoms along the first eigenvector, while the third row plots the probability density that the system occupies a particular configuration. The lowermost row shows the projections of the trajectory on planes defined by pairs of eigenvectors. The PCA data show that DNA strands in systems **I** and **II** have greater freedom of movement compared to strands in system **III**.

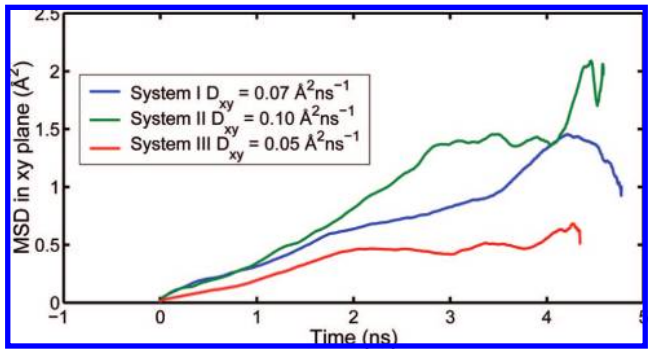

Figure 9. Mean-square displacement vs time graphs for DNA strands in all systems calculated from the production phase. The diffusion coefficients are found from the first half of the production phase as the accuracy of the calculation decreases at larger time scales. DNA strands in system **II** (Rüdorff) exhibit the greatest diffusion, while those in system **III** have the lowest mobility.

cations, so it is perhaps surprising that their diffusion coefficients are so large. Indeed, as previously noted, it suggests that peristaltic modes of motion may be driving some strands through the interlayer.

The PCA results of section 3.3 show that DNA strands in the Daumas−Hérold and Rüdorff arrangements have the greatest freedom of movement. However, the diameters of the DNA strands are, on average, more compressed in Rüdorff and stage-1 arrangements, which indicates that there is a greater force compressing the DNA and therefore restricting its movement. The RDF plots in Figure 7 show that phosphate groups in the Daumas−Hérold and Rüdorff models are surrounded by similar numbers of water molecules, while the phosphate groups in the stage-1 system have less. The stage-1 model also has the largest number of phosphate ions residing close to the LDH surface. These structural differences cause the DNA stacked in a stage-1 arrangement to be more confined in its motion compared to the Daumas−Hérold and Rüdorff arrangements.

Table 3. Diffusion Coefficients for Systems **I**, **II**, and **III**, Calculated from the First Half of the Production Phase of the Simulations[a]

diffusion coefficient D (Å^2 ns^{-1})	system **I** (Daumas−Hérold)	system **II** (Rüdorff)	system **III** (stage-1)
Max.	0.28 ± 0.01	0.28 ± 0.01	0.09 ± 0.01
Min.	0.00 ± 0.01	0.00 ± 0.01	0.00 ± 0.01
Average	0.07 ± 0.1	0.10 ± 0.1	0.05 ± 0.03

[a] In comparison, the diffusion coefficient for intercalated water molecules has been determined from simulation and experimental studies to be ∼1 Å^2 ns^{-1}.[21,65,66] Error bars are obtained from the least-squares fit error on the gradient of the mean-square displacement vs time graph. The variation in diffusion coefficients for all DNA molecules is greatest for the Daumas−Hérold and Rüdorff configurations, but on average DNA strands in the Rüdorff model show greatest mobility.

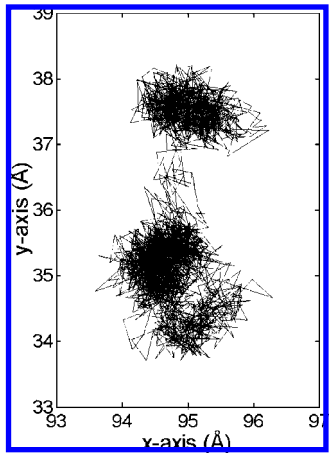

Figure 10. Superposition of 2434 spatial trajectories which follow the (x, y) coordinates of a phosphorus atom belonging to a DNA strand in system **I**, obtained during the 4.0 ns production phase of the simulation. The plot reveals the jump diffusion seen in some of the phosphate groups of the DNA strands, showing that the ionic phosphate groups spend the most time at charged sites where aluminum ions reside.

4. Conclusions

The simulations in this study have been used to investigate the various structural features apparent when linear dodecamer duplex strands of DNA are stacked in different arrangements while intercalated into $[Mg_2Al(OH)_6]Cl$ LDHs. The large-scale molecular dynamics techniques used in this study give insight into the intercalation structures and dynamics of layered materials; these are very hard to quantify in a comparable manner experimentally. Together with previous studies,[21,22,26] our simulations show that clay minerals are not rigid, nor are the host layers decoupled from the intercalant as far as adsorption mechanisms and kinetics are concerned.

When DNA strands occupy all interlayer regions but are stacked in a staggered conformation, we find that the LDH layers deform into a Daumas−Hérold configuration, as seen with graphite intercalation compounds.[4,15] However, even when DNA molecules are interstratified to form a Rüdorff configuration, LDH layers are able to bend around intercalants, albeit to a lesser extent.

In addition to hydration, the arrangement of DNA strands plays an important role in the structural stability of the intercalated DNA. Although all the systems are quite similar energetically, a staggered configuration of molecules has slightly lower potential energy than DNA molecules stacked directly on top of each other in a stage-1 configuration. Comparing structural properties of intercalated DNA with those for DNA in bulk water obtained in our earlier study,[26] we have found that DNA is least deformed from its conformation in bulk water, and has the largest percentage of intact Watson−Crick hydrogen bonds while in the Daumas−Hérold arrangement.

The diffusion of DNA within intragallery regions is an order of magnitude less than that of intercalated water molecules;[21] DNA is a relatively large, highly charged molecule compared to water. Diffusion coefficients were found to vary significantly between individual DNA strands in both the Daumas−Hérold and Rüdorff structures, which have, on average, the largest diffusion coefficients. The visualization evidence and spectral intensity analysis reveal that all models manifest peristaltic modes, which are more clearly defined in the Daumas−Hérold and stage-1 structures. However, the same diffusive motion of DNA is not present in the stage-1 system. This is most likely because peristaltic modes in the stage-1 structure are damped at shorter wavelengths compared to those in the Daumas−Hérold model. Therefore, our findings suggest that a Daumas−Hérold model promotes peristaltic modes which may be a cause of relatively high diffusion of some DNA strands.

Mean-field models of staging suggest that, in a Daumas−Hérold structure, intercalant islands within the same gallery may be attracted to one another, while islands in adjacent interlayers repel, providing a driving force for staging.[2,4] In our study, the manner in which DNA is intercalated influences its diffusion properties. While it is possible that the Daumas−Hérold scheme indeed promotes most rapid intercalation, longer and even more extensive simulation studies, preferably containing LDH models with edges, would be required to confirm these conclusions.

Acknowledgment. This work was supported by the UK Engineering and Physical Sciences Research Council (EPSRC, GR/T27488/01), which provided access to HPCx (www.hpcx.ac.uk), and by EPSRC grant GR/T04465/01 (ESLEA). We are indebted to the National Science Foundation for TeraGrid allocations under MRAC grant DMR070013N, utilizing resources on the US TeraGrid (www.teragrid.org) and the UK's National Grid Service (www.ngs.ac.uk). M.-A.T. was funded by an EPSRC Ph.D. studentship associated with the RealityGrid Project (GR/67699/02).

Supporting Information Available: Animations of the fluctuations in basal spacing with time for systems **I**−**III**. This material is available free of charge via the Internet at http://pubs.acs.org.

JA8037068